Supporting Information

Carbon nanopore and anchoring site-assisted general construction of encapsulated metal (Rh, Ru, Ir) nanoclusters for highly efficient hydrogen evolution in pH-universal electrolytes and natural seawater

Rong Ding [a], Tingting Yan [a], Yi Wang [a,*], Yan Long [a] and Guangyin Fan [a,*]

[a] College of Chemistry and Materials Science, Sichuan Normal University, Chengdu 610068, China

* Corresponding author
Email: wangyi@sicnu.edu.cn (Y. Wang); fanguangyin@scicnu.edu.cn (G. Fan)

Experimental section

Chemicals and Materials: Potassium hydrate and tetraethoxysilane (TEOS) were purchased from Alfa Aesar. Nafion and commercial Pt/C (20 wt%) were obtained from Sigma-Aldrich. Absolute ethanol and ammonia (25%) were provided by Kelong. Dopamine hydrochloride (DA). $RuCl_3 \cdot xH_2O$ (35.0 % Ru basis), $RhCl_3 \cdot xH_2O$ (39.5 % Rh basis), $H_2PtCl_6 \cdot 6H_2O$ (37.5 %) and $IrCl_3 \cdot xH_2O$ (54.35 % Ir basis) were purchased from Aladdin Reagent (China). Conductive carbon (Vulcan XC-72R) was obtained from Carbot Corp. All reagents were used without any purification and deionized water 18.2 MΩ cm were used in all reactions.

Synthesis of N-doped hollow carbon spheres (NHCSs): Firstly, DA/SiO_2 spheres were prefabricated by a facile one-step approach involving the formation of spherical SiO_2 cores and DA coating. In short, a mixed solution containing 1.0 mL of ammonia, 24.0 mL of absolute ethanol and 80.0 mL deionized water was vigorously stirred for 10 mins. 1.0 mL of tetraethoxysilane (TEOS) was added into the above mixture, and the stirring lasted for another 10 mins. Then, 50.0 mg mL^{-1} (8 mL) of DA solution was added into the aforesaid mixture solution and continuously stirring for 24 h. Brown deposition was collected after centrifugation and washed with distilled water several times. The as-formed DA/SiO_2 spheres were carbonized at 800 °C for 4 h under Ar flow with a heating rate of 5 °C min^{-1}. Then obtained sample was etched in 5.0 M potassium hydrate aqueous solution at 90 ℃ for 3 h to remove the SiO_2 template. After that, the N-doped hollow carbon spheres were obtained by centrifugation, washed follow with water and ethanol for several times and finally

dried at 60℃ for overnight.

Synthesis of M/NHCSs: The stock aqueous solution of MCl_3 (M= Ru, Rh, and Ir) with a concentration of 10 mg mL^{-1} was firstly prepared. Then, 25.0 mg NHCSs was added into 2.0 mL of deionized water and equably scattered by ultrasonication for 0.5 h. Afterward, the calculated amount of MCl_3 aqueous solution was added (500 μL $RuCl_3$ for Ru/NHCSs, 320 μL $IrCl_3$ for Ir/NHCSs, and 443 μL $RhCl_3$ for Rh/NHCSs, respectively). The mixture in the beaker was stirred by a magnetic stirrer for 12 h at room temperature. The samples were dried at 80 ℃ under vacuum overnight and then reduced in 5% H_2/Ar atmosphere (50 mL min^{-1}) at 300 ℃ for 2 h.

Synthesis of Pt/NHCSs: The synthesis method of Pt/NHCSs was the same as that of M/NHCSs, except that the 470 μL $H_2PtCl_6 \cdot 6H_2O$ was added.

Synthesis of Rh/C: The synthesis method of Rh/C was the same as that of Rh/NHCSs, except that NHCSs was replaced by conductive carbon (Vulcan XC-72R).

Characterization: X-ray diffraction (XRD) was executed on a Regaku D/Max-2500 diffractometer. Transmission electron microscopy (TEM, JEM-2100F, JEOL) was used to measure the morphology and microstructure of Rh/NHCSs and the other three samples. Generally, 150 spots were measured to calculate the size of metal nanoclusters in each sample. The surface elements and chemical valence of the catalyst were detected by X-ray photoelectron spectroscopy on a Thermo ESCALAB 250 Axis Ultra spectrometer. N_2 sorption measurement was performed on an Automated Gas Sorption Analyzer (Quanta Autosorb-IQ). The pore size distributions of the samples were calculated based on the density functional theory (DFT) method.

SEM-Mapping and Energy dispersive X-ray spectroscopy (EDX) was conducted on Oxford instrument operating at 200 kV. Inductively coupled plasma-optical emission spectrometry (ICP-OES) analysis was carried out on SPECTRO ARCOS spectrometer.

Electrochemical measurements: The electrochemical measurements were carried out on an electrochemical workstation (CHI 760E). All HER measurements were carried out on a standard three-electrode system which consists of a glass carbon (GC) rotating disk electrode (RDE) (d=4 mm) as the working electrode, Hg/HgO (saturated calomel) as the reference electrode, and graphite rod as the counter electrode. To prepare the working electrode (WE): 2.0 mg of catalyst was added into the solution containing 990.0 μL of ethanol and 10.0 μL of 5% Nafion, and the mixture was ultrasonically dispersed 30 min to form a uniform suspension. Afterward, 40.0 μL of catalyst ink was loaded as evenly as possible on the GC (0.1256 cm^2). The catalyst loading on the working electrode is about 636.9 μg cm^{-2}. All the linear sweep voltammetry (LSV) curves were represented with iR-compensation. The scan rate was 5 mV s^{-1} for linear sweep voltammetry tests and long-term cyclic voltammetry tests.

The electrolytes were 0.5 M H_2SO_4, 1.0 M PBS and 1.0 M KOH. For seawater electrolysis, natural seawater (pH= 8.35) was taken from Beidaihe (China), which was filtered to remove deposition before use. The main composition of natural seawater was measured follows:

Substances	Mass (g/kg)	Percentage (%)

Sodium chloride	27.2	77.7
Magnesium chloride	3.8	10.9
Magnesium sulfate	1.7	4.9
Calcium sulfate	1.2	3.6
Potassium sulfate	0.9	2.5
Calcium carbonate	0.1	0.3
Magnesium bromide and others	0.1	0.3

In all measurements, the potential was calibrated to the reversible hydrogen electrode (RHE) according to the following Nernst equation:

1) In 0.5 M H_2SO_4 and 1.0 M PBS , E (RHE)= E (SCE)+0.059×pH;
2) In 1.0 M KOH E (RHE) = E (vs Hg/HgO) + 0.059×pH.

The overpotential was calculated as follows:

η= E (vs. RHE) –E^0 (vs. RHE)

Where η, E, and E^0 denote the overpotential, actual applied potential, and reversible potential of the reaction, respectively. E^0 is 0 V for the HER[1].

Turnover Frequency Calculation[2, 3]:

The TOF of M/NHCSs can be determined from the following general equation:

$$TOF=j/(2*n(M,s)*F) \quad (1)$$

where j is the measured current density at a given overpotential (A cm^{-2}), F is the Faraday constant (96485 C mol^{-1}), the factor 2 refers to 2 electrons required to

produce one H_2 molecule and n(M, s) is the number of moles of active M sites per geometric surface area (mol cm^{-2}). If we assume that all M atoms in the M/NHCSs catalyst are exposed to the solution and available for the HER, then we can calculate n(M, s) from the following equation:

$$n(M,s) = x(M)*n(catalyst,s) = x(M)*(catalyst\ loading)/M(catalyst) \qquad (2)$$

where x(M) is the mole fraction of M in the catalyst, n(catalyst, s) is the total amount of the M/NHCSs catalyst per geometric surface area (mol cm^{-2}), the catalyst loading is $4.2*10^{-4}$ g cm^{-2} and M (catalyst) is the relative molar mass of the catalyst (g mol^{-1}) which can be obtained from:

$$M(catalyst) = x(M)*M(M) + x(O)*M(O) + x(C)*M(C) + x(N)*M(N) \qquad (3)$$

In the above equation x(M), x(O), x(N) and x(C) are the mole fractions of M, O ,N and C, respectively, and they can be taken as the atomic percentages that are determined from the XPS analysis, while M(M), M(O), M(N) and M(C) are the corresponding molar masses. After inserting Equations (2) and (3) in (1), we obtain the final equation for TOF calculation:

$$TOF=j/(2*x(M) * (catalyst\ loading) *F/(x(M) *M(M) + x(O) *M(O) + x(C) *M(C) + x(N) *M(N))). \qquad (4)$$

Surface metal atoms on three samples were measured from XPS data (atomic percentage):

Ru/NHCSs: Ru: 4.85%, C: 81.64%, O: 8.85%, N: 4.66%,

Rh/NHCSs: Rh: 0.75%, C: 88.10%, O: 5.65%, N: 5.60%,

Ir/NHCSs: Ir: 0.36%, C: 86.10%, O: 7.30%, N: 6.24%.

In Ru/NHCSs catalyst:

M (Ru/NHCSs) = 101.1 g mol^{-1}×4.85%+12.01 g mol^{-1}×81.64%+16.00 g mol^{-1}×8.85%+14.00 g mol^{-1}×4.66% = 16.78 g mol^{-1}

n (Ru) = 4.85%×4.2×10^{-4} g cm^{-2}/(16.78 g mol^{-1}) = 1.2×10^{-6} mol cm^{-2}

The HER current density at an overpotential of 30 mV is 0.01279 A cm^{-2} for Ru /NHCSs. The TOF of Ru /NHCSs was calculated to be:

TOF = 0.01279 A cm^{-2}/ (2×1.2×10^{-6} mol cm^{-2}×96485C mol^{-1}) =0.06 s^{-1}

In Rh/NHCSs catalyst:

M (Rh/NHCSs) = 102.9 g mol^{-1}×0.75%+12.01 g mol^{-1}×88.10%+16.00 g mol^{-1}×5.65%+14.00 g mol^{-1}×5.60% = 13.04 g mol^{-1}

n (Rh) = 0.75%×4.2×10^{-4} g cm^{-2}/(13.04 g mol^{-1}) = 2.42×10^{-7} mol cm^{-2}

The HER current density at an overpotential of 30 mV is 0.0633 A cm^{-2} for Rh /NHCSs. The TOF of Rh /NHCSs was calculated to be:

TOF = 0.0633 A cm^{-2}/ (2×2.42×10^{-7} mol cm^{-2}×96485C mol^{-1}) =1.4 s^{-1}

In Ir/NHCSs catalyst:

M (Ir/NHCSs) = 192.2 g mol^{-1}×0.36%+12.01 g mol^{-1}×86.10%+16.00 g mol^{-1}×7.30%+14.00 g mol^{-1}×6.24% = 13.07 g mol^{-1}

n (Ir) = 0.75%×4.2×10^{-4} g cm^{-2}/(13.07 g mol^{-1}) = 1.16×10^{-7} mol cm^{-2}

The HER current density at an overpotential of 30 mV is 0.0066 A cm^{-2} for Rh /NHCSs. The TOF of Rh /NHCSs was calculated to be:

TOF = 0.0066 A cm^{-2}/ (2×1.16×10^{-7} mol cm^{-2}×96485C mol^{-1}) =0.29 s^{-1}

The TOF values for Ru/NHCSs, Rh/NHCSs, Ir/NHCSs in 1.0 M PBS and 0.5 M H_2SO_4 were calculated in the same way as the above calculation (shown in Table S4).

Mass activity Calculation:

The following formula was used to calculate the Mass activity of the samples:

Mass activity = $current\ density/$percent of metal mass × catalyst loading of working electrode

The noble metal content of three samples were measured by IPC (mass percent):

Ir/NHCSs: Ir: 6.14 wt%,

Rh/ NHCSs: Rh: 6.54 wt%,

Ru/NHCSs: Ru: 6.35 wt%.

In 1.0 M KOH, the current density at the overpotential of 20 mV is 4.81 mA cm^{-2} for Ir/NHCSs.

The mass activity of Ir/NHCSs was calculated as:

$$Mass\ activity = \frac{4.84\ mA\ cm^{-2}}{6.14\ wt\% \times 4.2 \times 10^{-4} g\ cm^{-2}} = 187.7\ A\ g^{-1}$$

The current density at the overpotential of 20 mV is 37.05 mA cm^{-2} for Rh/NHCSs.

The mass activity of Rh/NHCSs was calculated as:

$$Mass\ activity = \frac{37.05\ mA\ cm^{-2}}{6.54\ wt\% \times 4.2 \times 10^{-4} g\ cm^{-2}} = 1348.5\ A\ g^{-1}$$

The current density at the overpotential of 20 mV is 8.49 mA cm^{-2} for Ru/NHCSs. The mass activity of Ru/NHCSs was calculated as:

$$Mass\ activity = \frac{8.49\ mA\ cm^{-2}}{6.35\ wt\% \times 4.2 \times 10^{-4} g\ cm^{-2}} = 318.3\ A\ g^{-1}$$

The mass activity of Ru/NHCSs, Rh/NHCSs, Ir/NHCSs in 1.0 M PBS and 0.5 M H_2SO_4 were calculated in the same way as the above calculation (the results shown in Table S3).

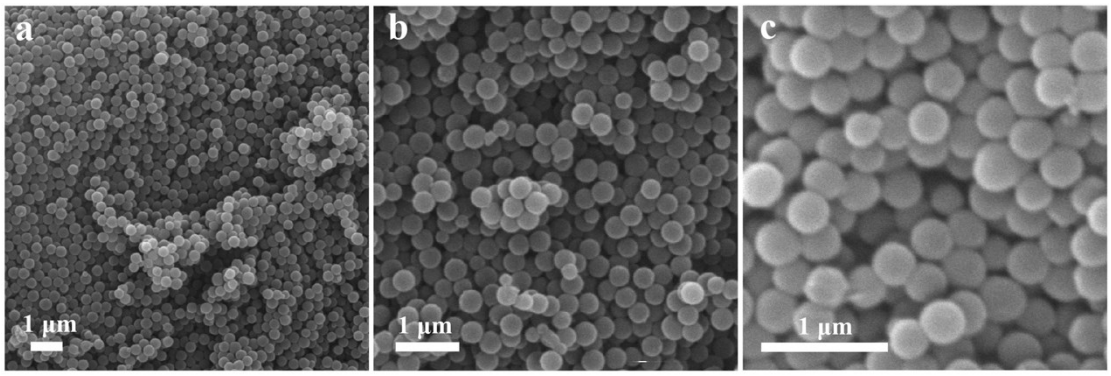

Fig. S1 SEM images of N-doped carbon spheres before etching.

N-doped carbon spheres were composed of uniform nanospheres with a diameter of ~290 nm and relatively smooth surface.

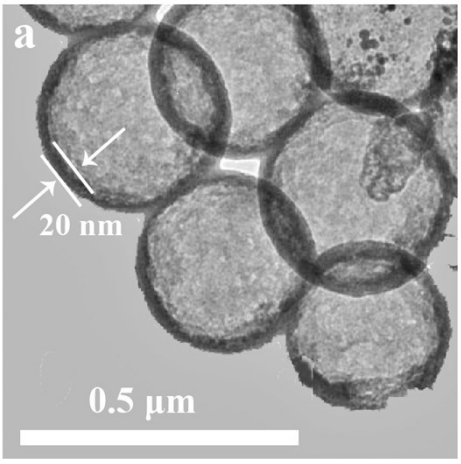

Fig. S2 TEM image of NHCSs.

After etching by KOH, uniform NHCSs with the thickness of 20 nm for carbon shell and 270 nm for carbon cavity were clearly observed.

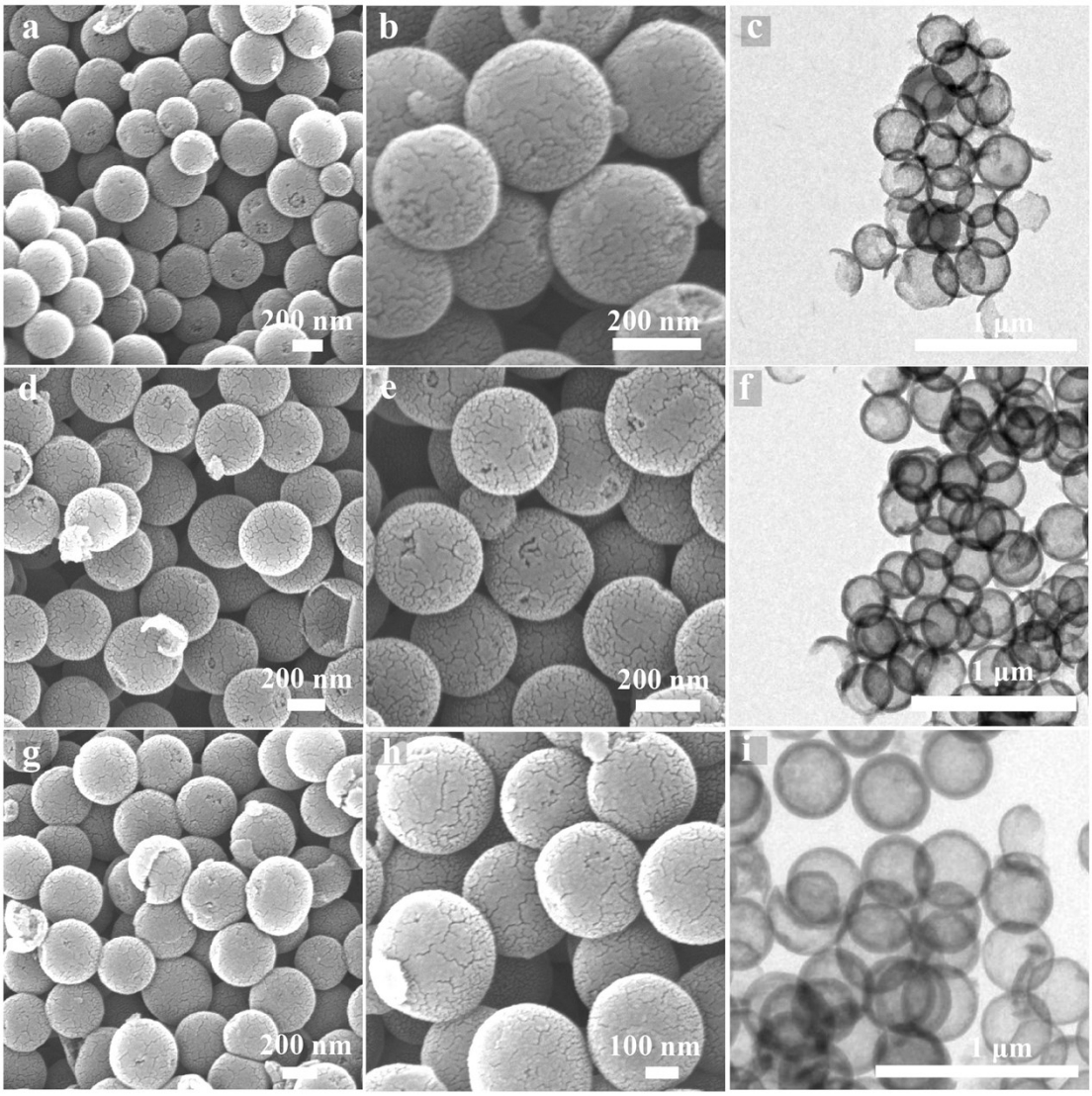

Fig. S3 SEM and TEM images of (a–c) Ru/NHCSs, (d–f) Rh/NHCSs, (g–i) Ir/NHCSs The surface of NHCSs became rougher after the loading of metal nanoclusters (MNCs) compared with pristine NHCSs, while the uniform hollow spherical morphology of the NHCSs maintained well.

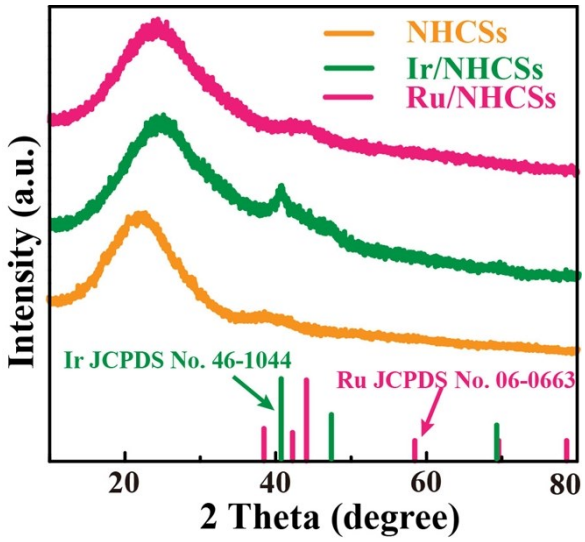

Fig. S4 XRD patterns of NHCSs, Ru/NHCSs and Ir/NHCSs.

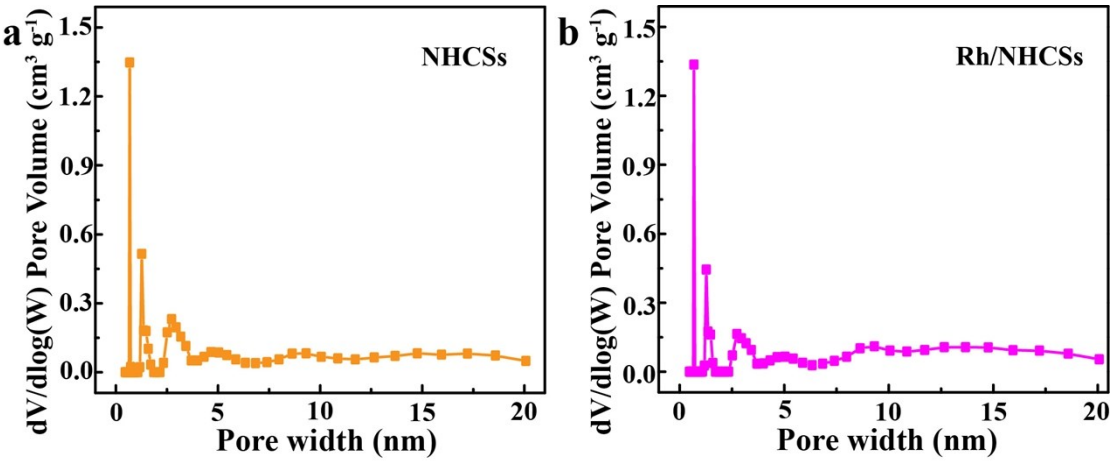

Fig. S5 The pore size distributions of (a) NHCSs and (b) Rh/NHCSs.

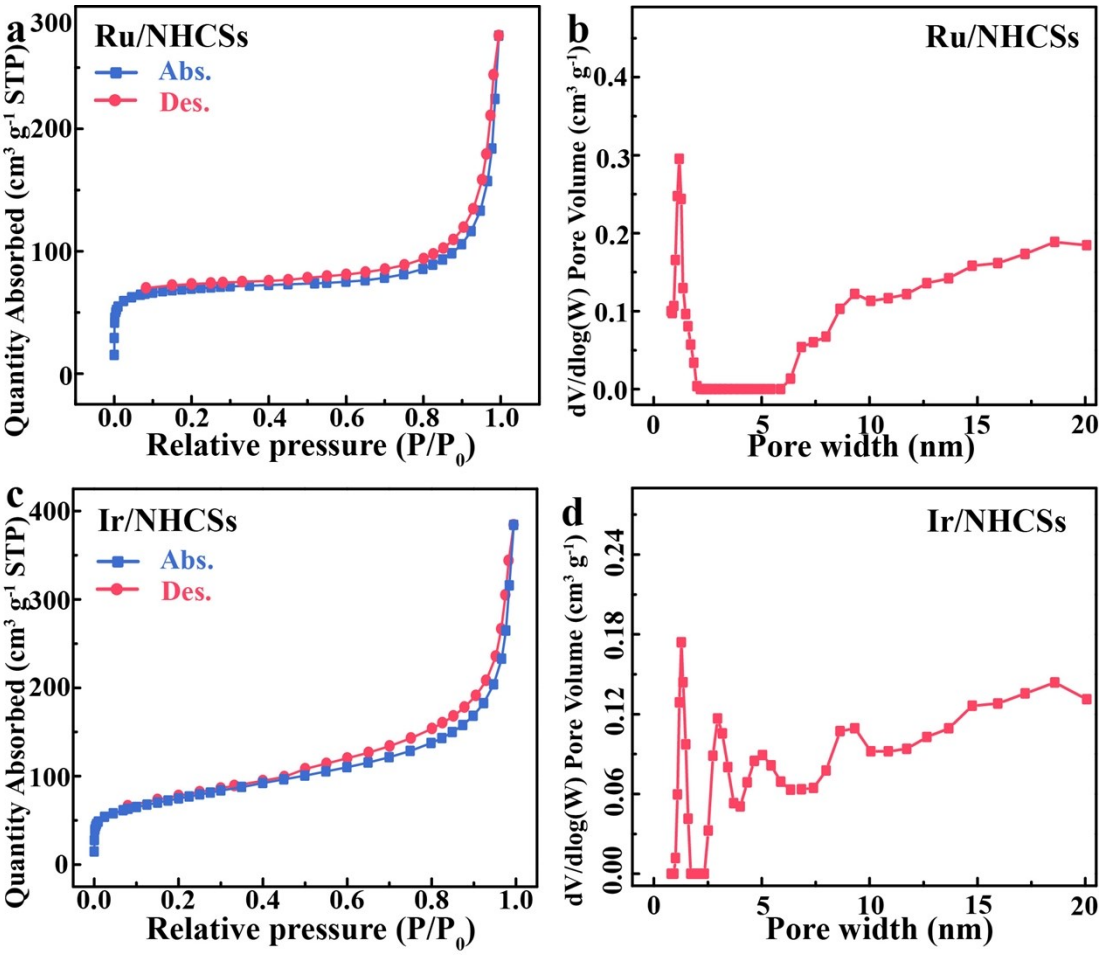

Fig. S6 N_2 sorption isotherm curves of (a) Ru/NHCSs and (c) Ir/NHCSs. The pore size distributions of (b) Ru/NHCSs and (d) Ir/NHCSs.

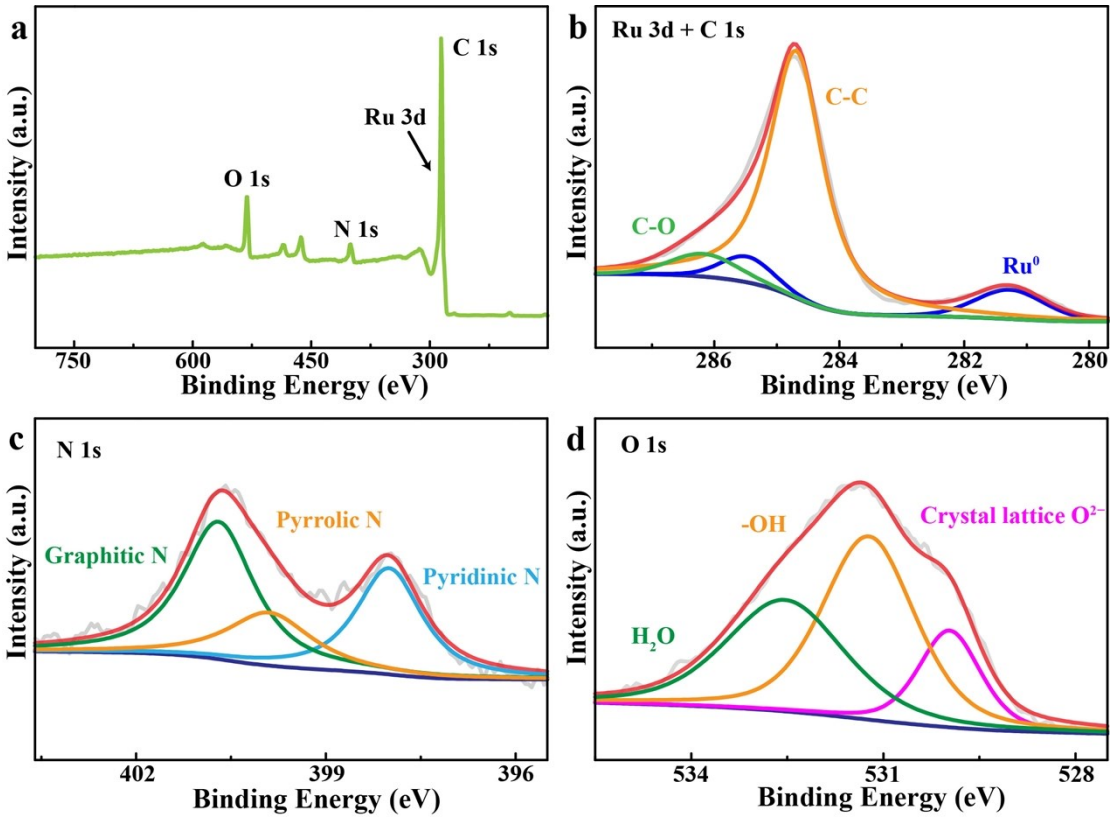

Fig. S7 (a) XPS survey and high-resolution XPS spectra of (b) Ru 3d, (c) N 1s and (d) O 1s for Ru/NHCSs.

The survey spectra of Ru/NHCSs indicated the presence of Ru, C, O and N across the samples. The coexistence of metallic Ru specie was observed by the fitted peaks from the spectra of Ru 3d in Ru/NHCSs.

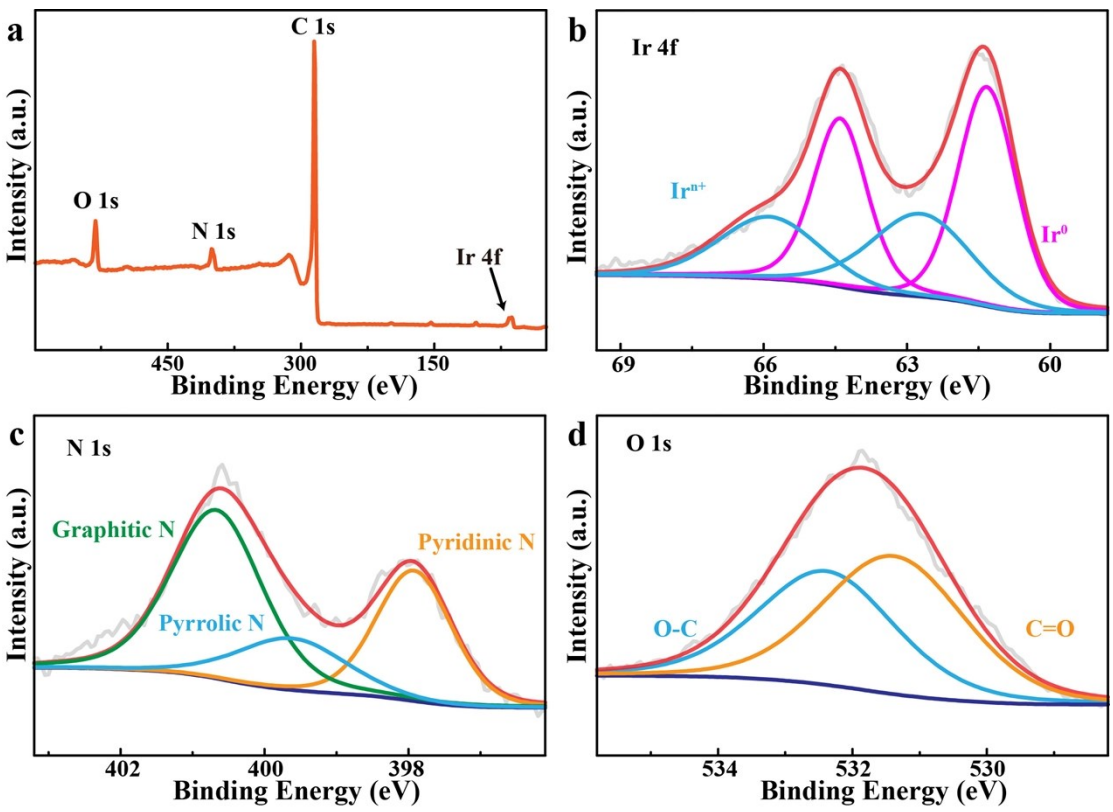

Fig. S8 (a) XPS survey and high-resolution XPS spectra of (b) Ir 3d, (c) N 1s and (d) O 1s for Ir/NHCSs.

The survey spectra of Ir/NHCSs indicated the presence of Ir, C, O and N across the samples. The coexistence of metallic and oxidized Ir species were observed by the fitted peaks from the spectra of Ir 4f in Ir/NHCSs.

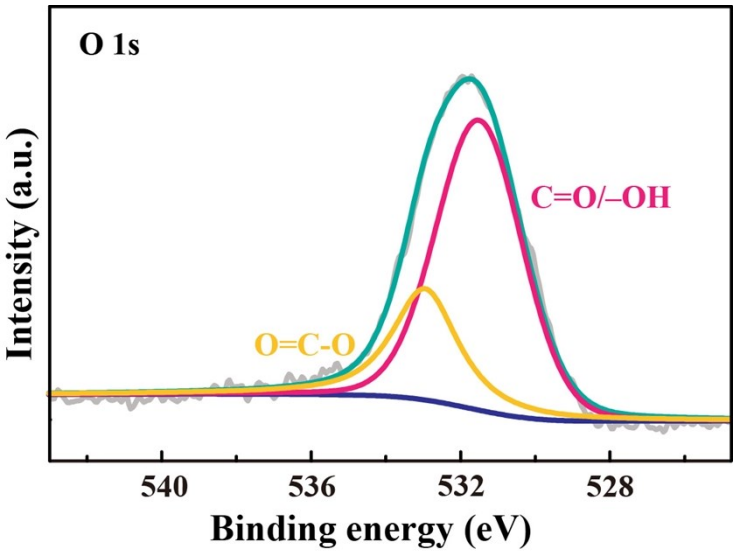

Fig. S9 The high-resolution XPS spectrum of O1s for Rh/NHCSs.

The O analysis by XPS, the deconvoluted O 1s spectra exhibited two components attributing to C=O/–OH and O=C-O groups (Fig. S6). These groups may play a synergistic role in charge separation and transfer[4, 5].

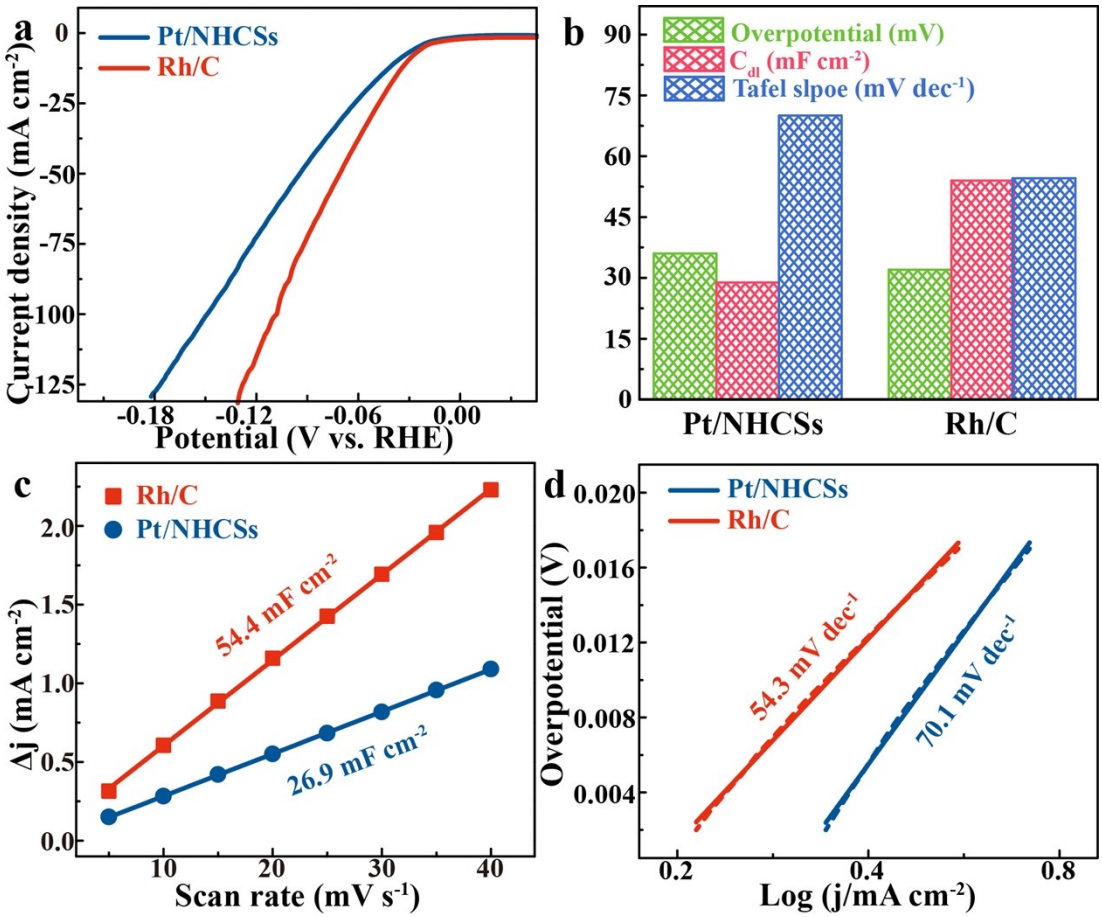

Fig. S10 (a) Polarization curves of Rh/C and Pt/NHCSs in 1.0 M KOH and (b) Overpotential, C_{dl} values, and Tafel slopes for Rh/C and Pt/NHCSs. (c) Capacitive current at the middle potential of CV curves as a function of scan rates and (d) Tafel plots and for Rh/C and Pt/NHCSs.

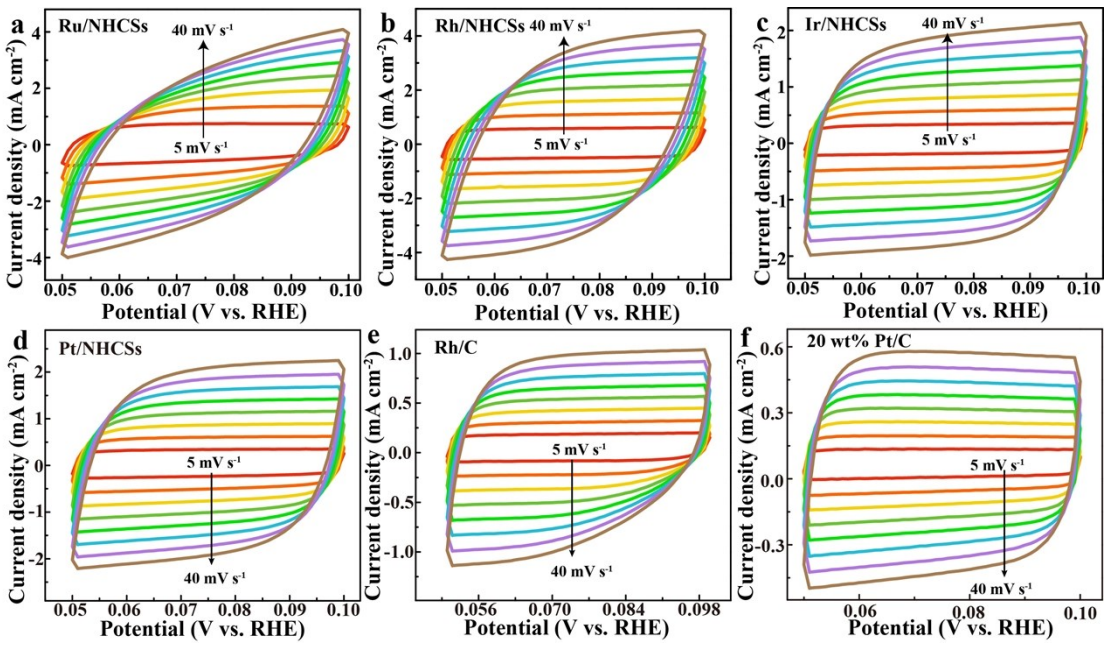

Fig. S11 CV curves measured at different scan rates from 5 to 40 mV s^{-1} in 1.0 M KOH for (a) Ru/NHCSs, (b) Rh/NHCSs, (c) Ir/NHCSs, (d) Pt/NHCSs, (e) Rh/C and (f) 20 wt% Pt/C.

.

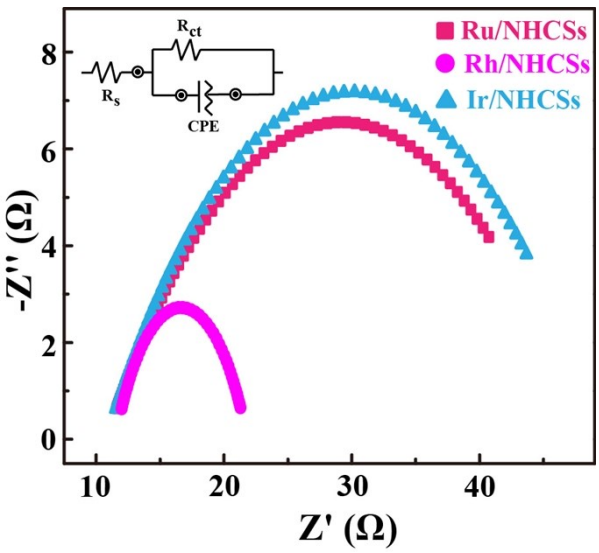

Fig. S12 EIS Nyquist plots at overpotential of 20 mV for Rh/NHCSs, Ru/NHCSs and Ir/NHCSs.

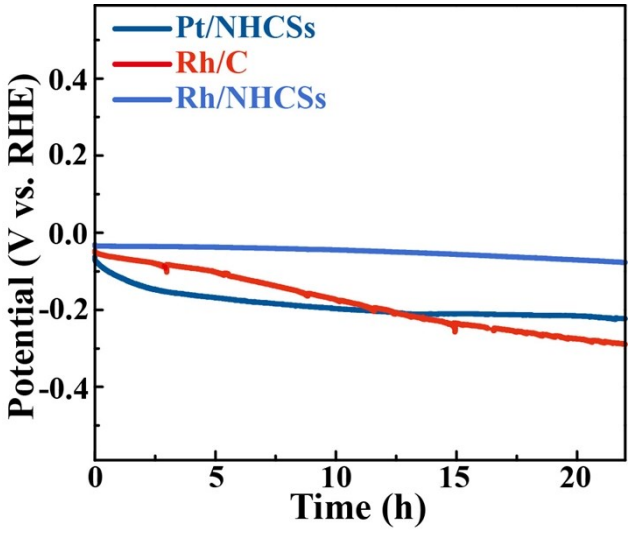

Fig. S13 V–t curves at 10 mA cm^{-2} for Pt/NHCSs, Rh/C and Rh/NHCSs in 1.0 M KOH.

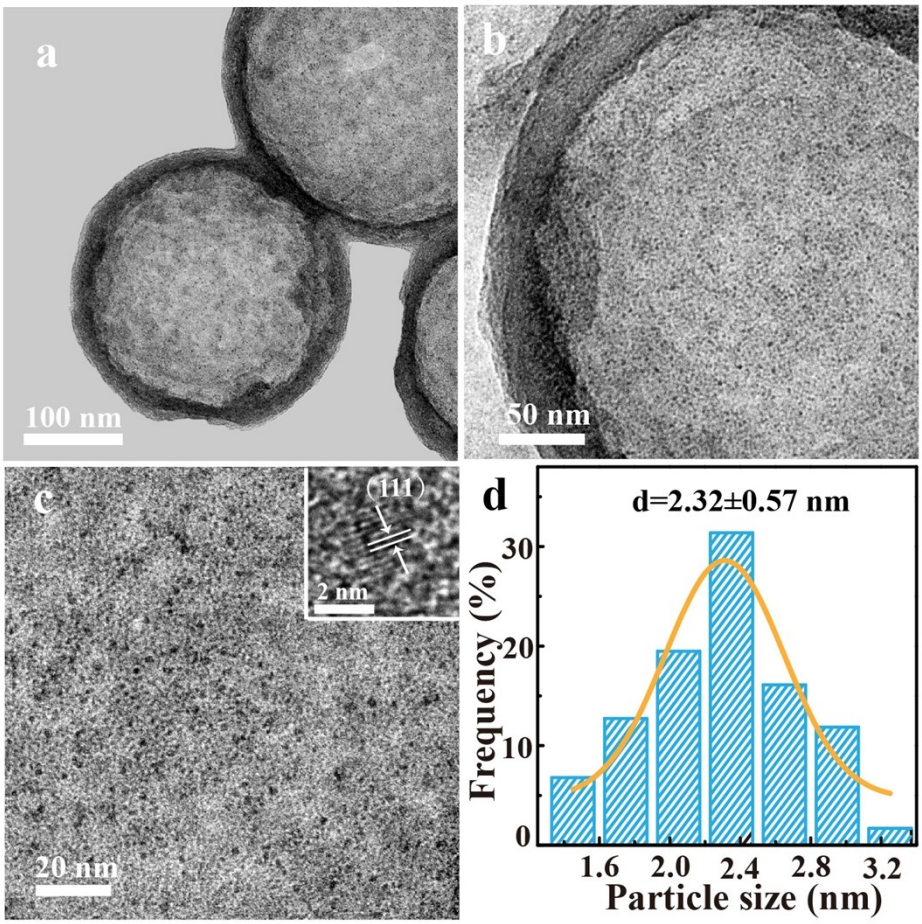

Fig. S14 (a–c) TEM images of Rh/NHCSs, and (d) size distribution of Rh NPs after 22 h V-t in 1.0 M KOH. The inset in (c) is the HRTEM image of Rh NPs.

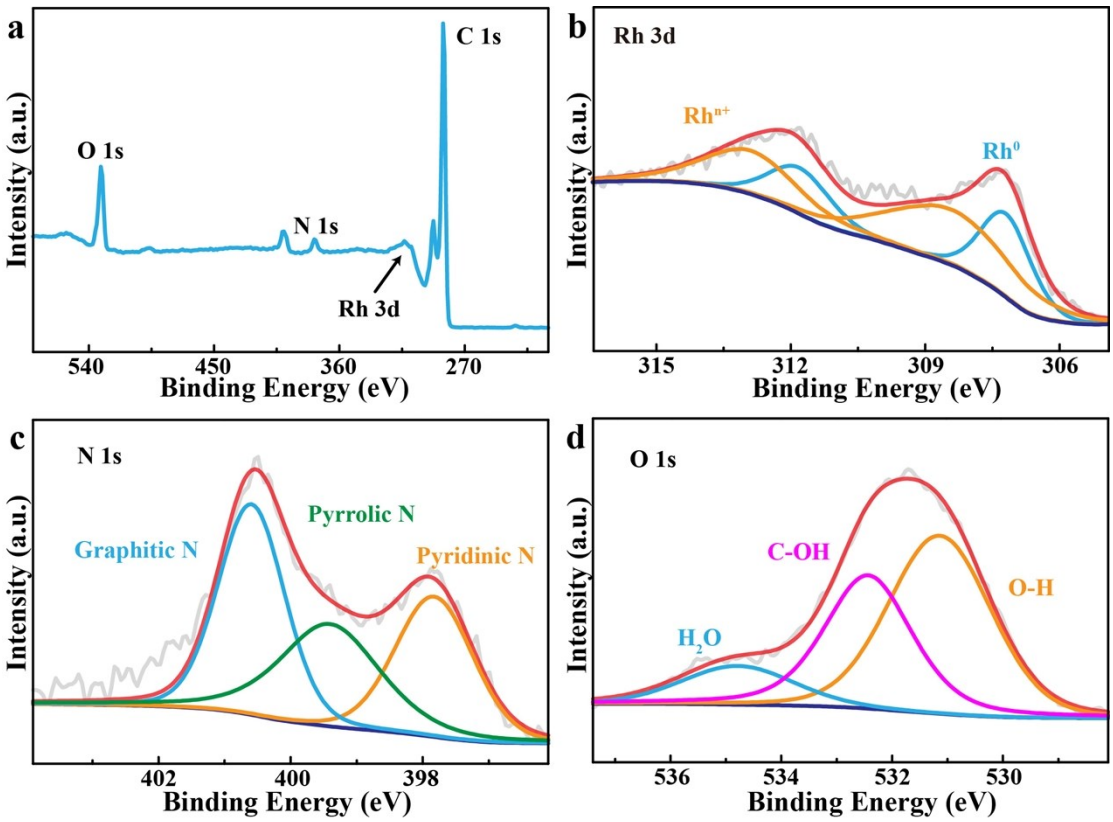

Fig. S15 (a) XPS survey and high-resolution XPS spectra of (b) Rh 3d, (c) N 1s and (d) O 1s for Rh/NHCSs after more than 20 h V-t test.

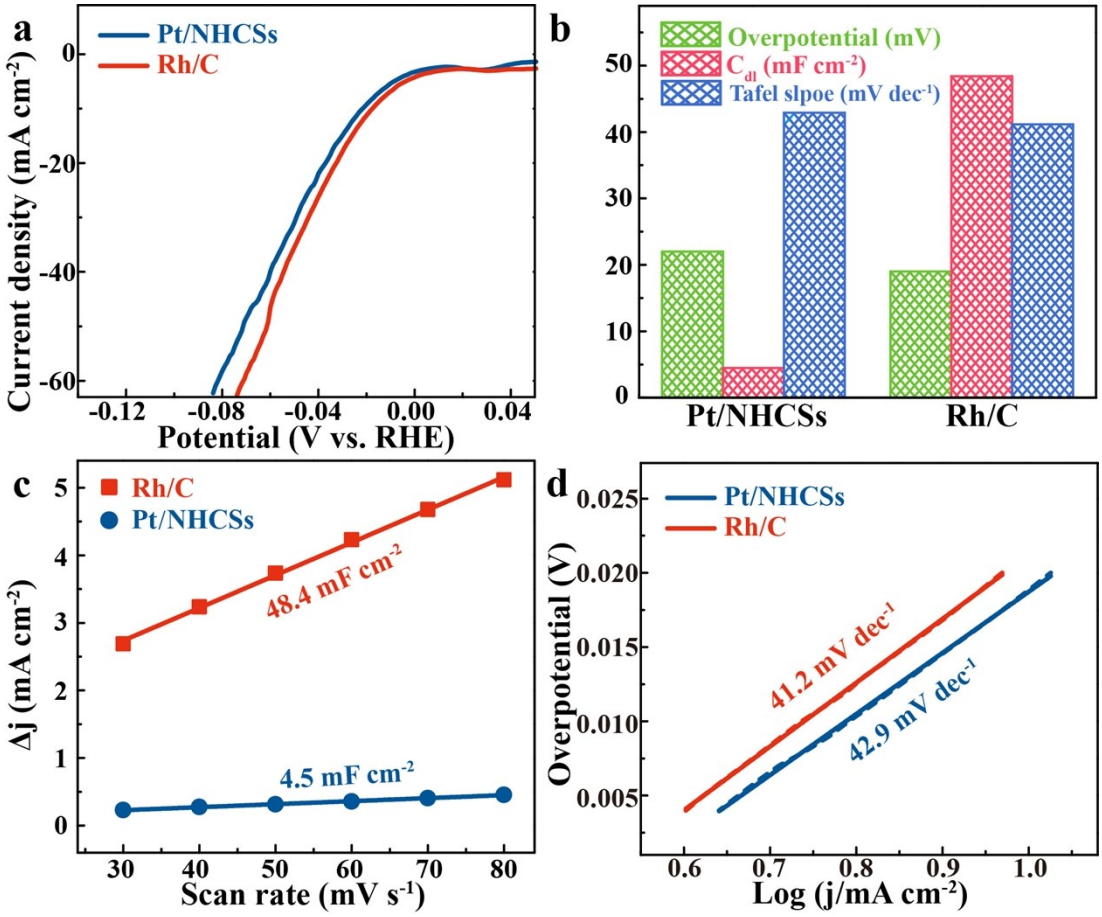

Fig. S16 (a) Polarization curves of Rh/C and Pt/NHCSs in 0.5 M H_2SO_4 and (b) Overpotential, C_{dl} values, and Tafel slopes for Rh/C and Pt/NHCSs. (c) Capacitive current at the middle potential of CV curves as a function of scan rates and (d) Tafel plots and for Rh/C and Pt/NHCSs.

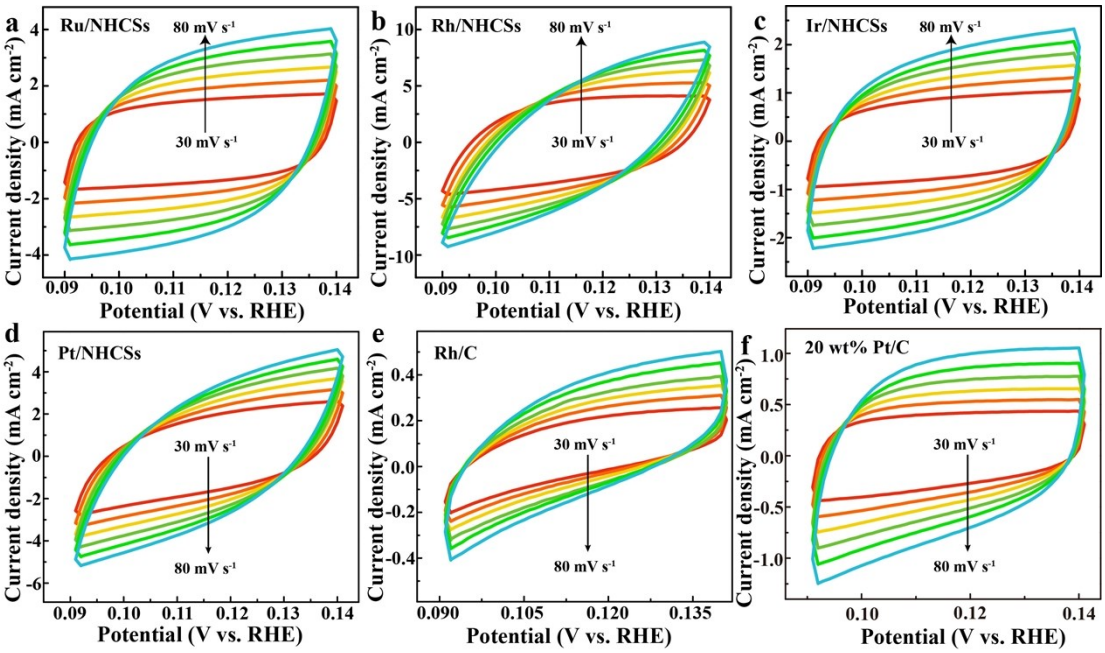

Fig. S17 CV curves measured at different scan rates from 30 to 80 mV s^{-1} in 0.5 M H_2SO_4 for (a) Ru/NHCSs, (b) Rh/NHCSs, (c) Ir/NHCSs, (d) Pt/NHCSs, (e) Rh/C and (f) 20 wt% Pt/C.

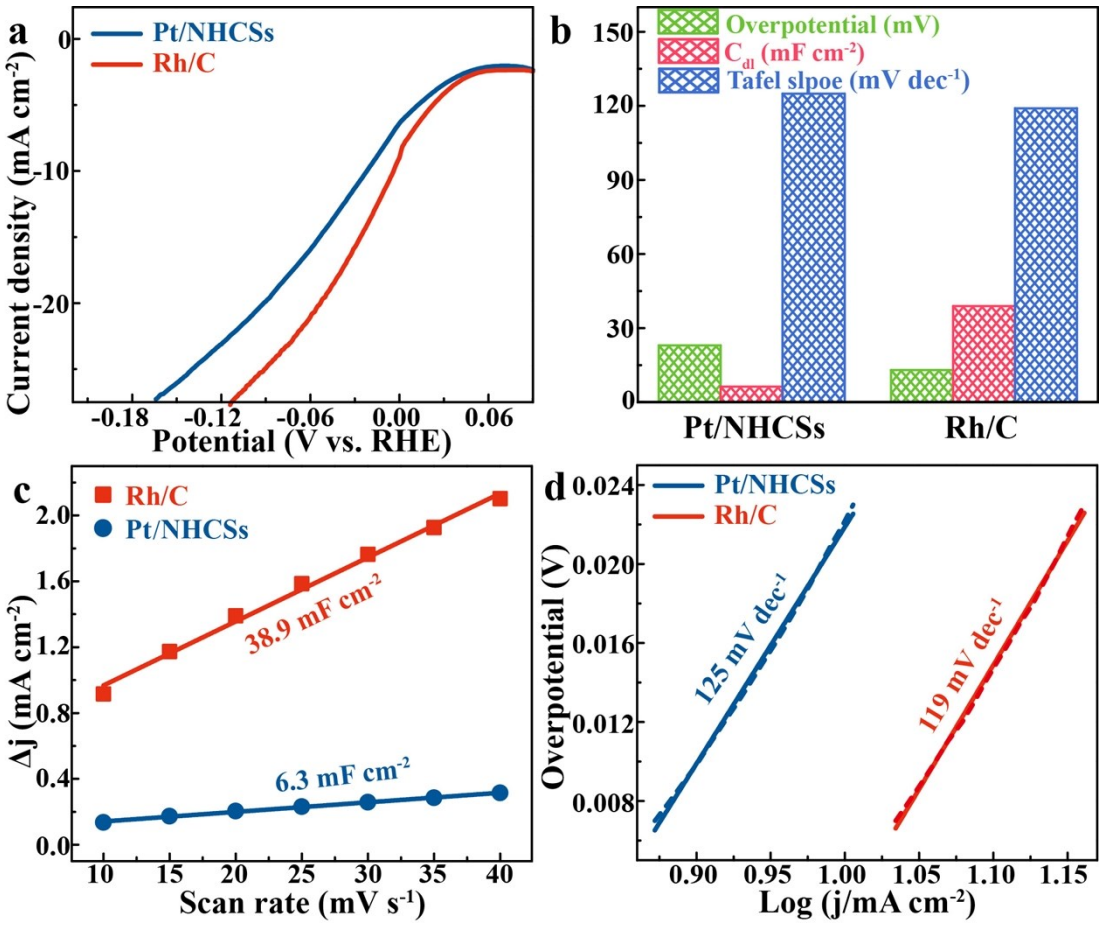

Fig. S18 (a) Polarization curves of Rh/C and Pt/NHCSs in 1.0 M PBS and (b) Overpotential, C_{dl} values, and Tafel slopes for Rh/C and Pt/NHCSs. (c) Capacitive current at the middle potential of CV curves as a function of scan rates and (d) Tafel plots and for Rh/C and Pt/NHCSs.

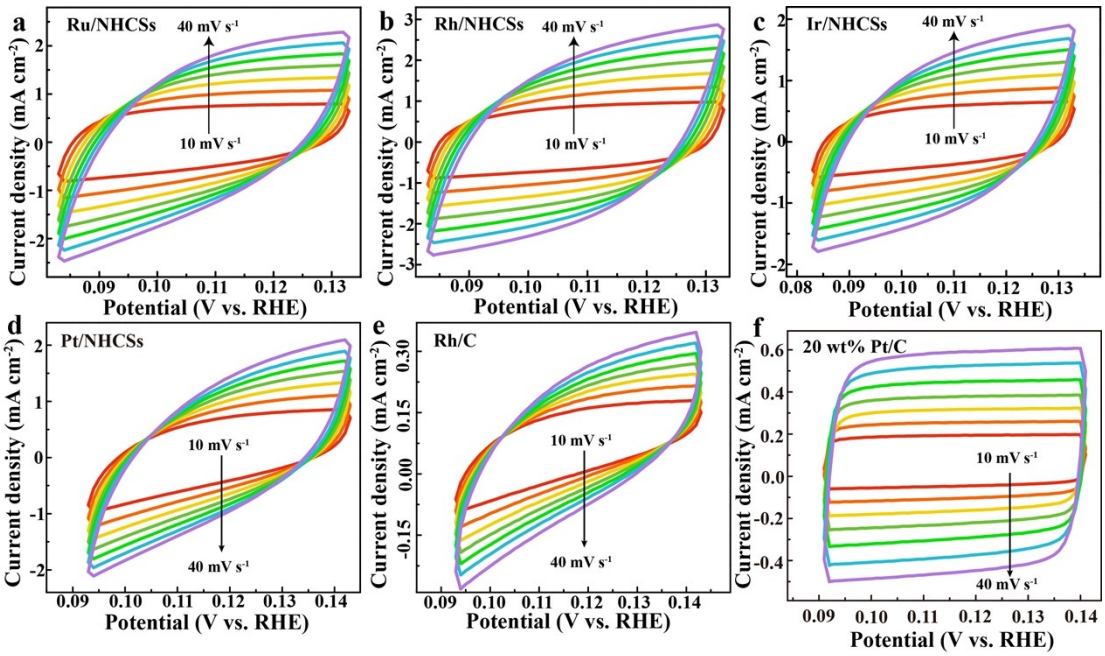

Fig. S19 CV curves measured at different scan rates from 10 to 40 mV s^{-1} in 1.0 M PBS for (a) Ru/NHCSs, (b) Rh/NHCSs, (c) Ir/NHCSs, (d) Pt/NHCSs, (e) Rh/C and (f) 20 wt% Pt/C.

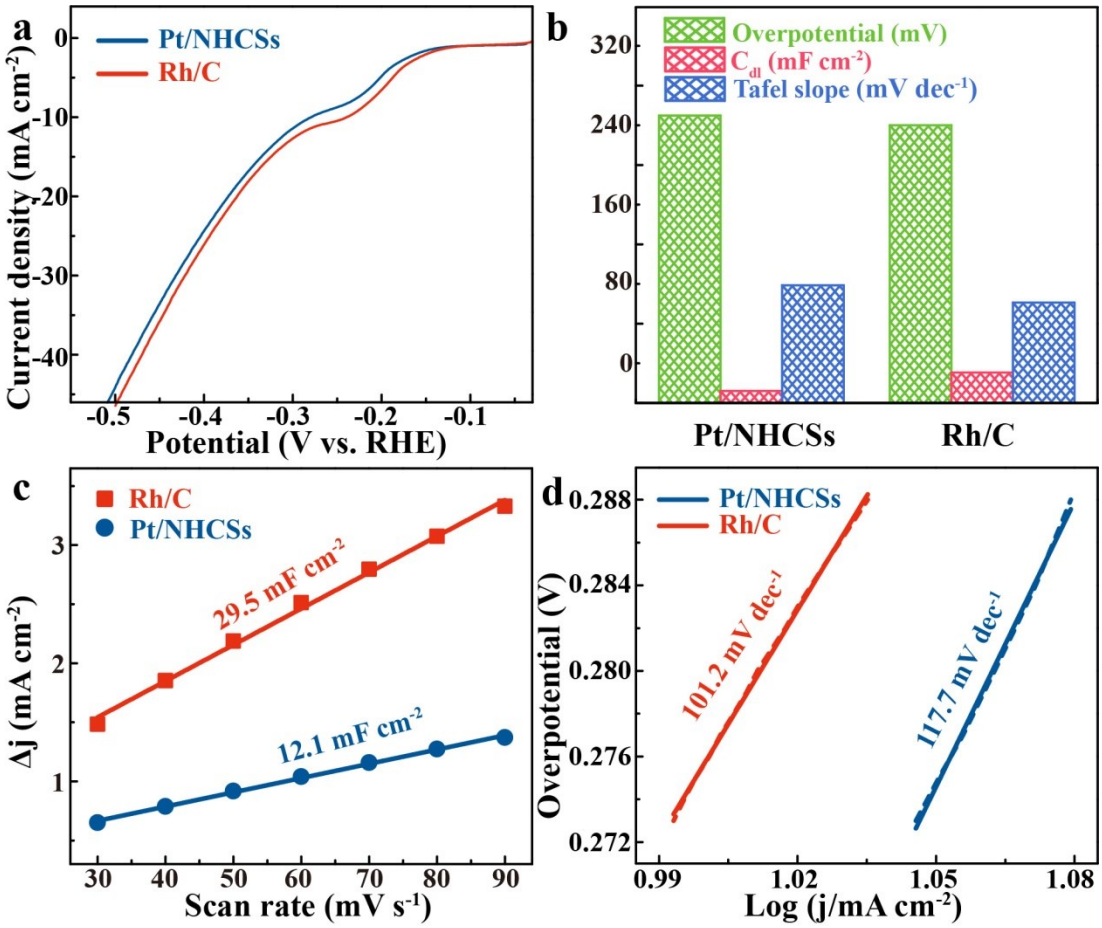

Fig. S20 (a) Polarization curves of Rh/C and Pt/NHCSs in natural seawater and (b) Overpotential, C_{dl} values, and Tafel slopes for Rh/C, Pt/NHCSs. (c) capacitive current at the middle potential of CV curves as a function of scan rates and (d) Tafel plots for Rh/C and Pt/NHCSs.

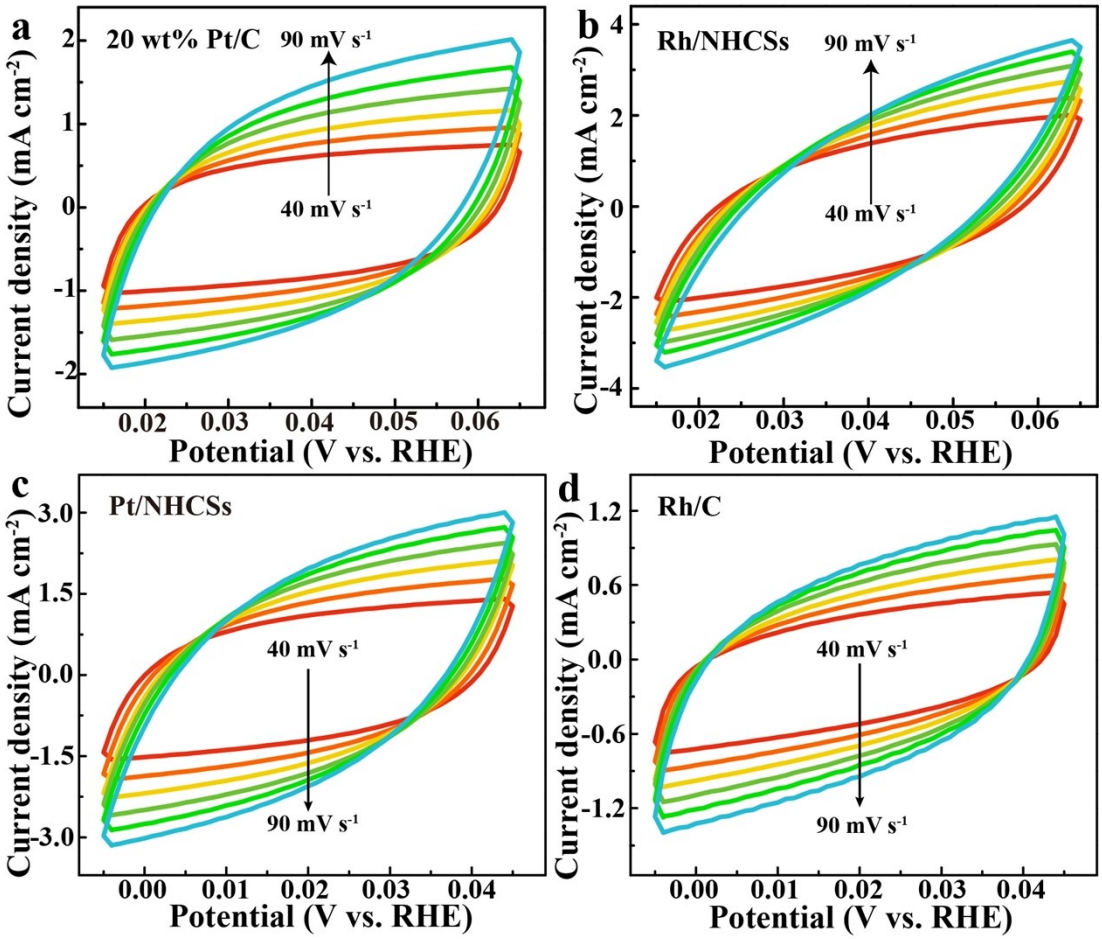

Fig. S21 CV curves measured at different scan rates from 40 to 90 mV s^{-1} in natural seawater for (a) 20 wt% Pt/C, (b) Rh/NHCSs, (c) Pt/NHCSs and (d) Rh/C.

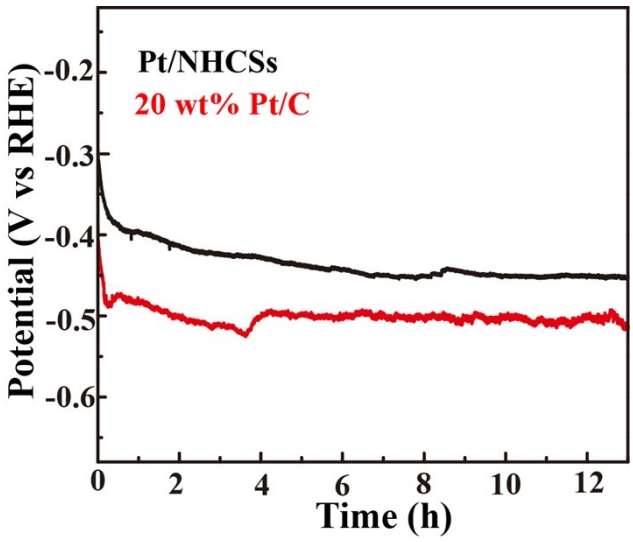

Fig. S22 V–t curves at 10 mA cm^{-2} for Pt/NHCSs and 20 wt % Pt/C in seawater.

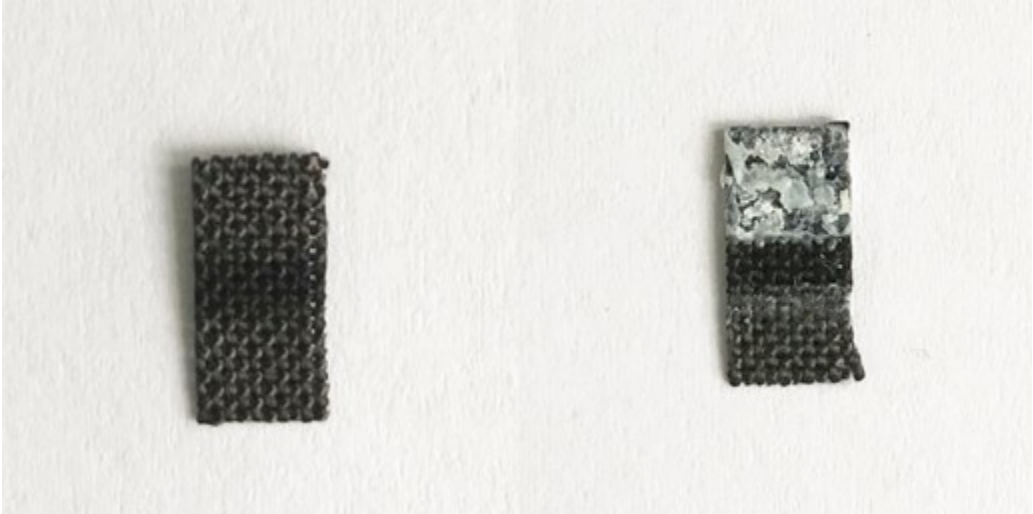

Fig. S23 Photograph of carbon cloth before and after cycling in natural seawater. Many precipitates were formed on the carbon cloth after the durability test.

Table S1. XPS analyses and surface structure properties of NHCSs, Rh/NHCSs, Ru/NHCSs and Ir/NHCSs.

Catalysts	N (At %)	C (At %)	O (At %)	$S_{BET}(m^2g^{-1})$	$V_{micro}(cm^3g^{-1})$
NHCSs	7.04	89.07	3.89	637.9	0.081
Rh/NHCSs	5.60	88.10	5.65	563.4	0.075
Ru/NHCSs	4.66	81.64	8.85	263.9	0.079
Ir/NHCSs	6.24	86.10	7.30	267.1	0.043

The result shows that after the loading of the different metals, the N content decreased but the O increased. The O analysis by XPS, the deconvoluted O 1s spectra exhibited two components attributing to C=O/–OH and O=C-O groups (Figs. S4d, S5d and S6). These groups may play a synergistic role in charge separation and transfer[4, 5]. As illustrated in Table S1, the O content of M (M=Ru, Ir)/NHCSs higher than Rh/NHCSs. The excessive oxygen moieties might be unfavorable to the electron transfer oxidation[6].

Table S2. HER properties of Rh/NHCSs, Ru/NHCSs Ir/NHCSs, Pt/NHCSs and Rh/C.

Catalysts	Electrolyte	Overpotential @10 mA cm^{-2} (mV)	C_{dl} (mF cm^{-2})	Tafel slope (mV dec^{-1})
Rh/NHCSs	1.0 M KOH	6	103.4	23.8
	1.0 M PBS	7	62.4	95.5
	0.5 M H_2SO_4	10	93.9	29.6
	Seawater	220	30.5	23.4
Ru/NHCSs	1.0 M KOH	26	92.9	54.1
	1.0 M PBS	36	52.1	101.4
	0.5 M H_2SO_4	47	47.6	92.6
Ir/NHCSs	1.0 M KOH	45	50.4	79.8
	1.0 M PBS	59	40.5	121.8
	0.5 M H_2SO_4	61	25.5	133
Pt/NHCSs	1.0 M KOH	36	28.86	70.06
	1.0 M PBS	23	6.3	125
	0.5 M H_2SO_4	22	4.47	42.9
	Seawater	290	12.07	118.7
Rh/C	1.0 M KOH	32	54	54.3
	1.0 M PBS	13	38.9	119
	0.5 M H_2SO_4	19	48.4	41.16
	Seawater	280	29.5	101.2

Table S3. Comparison of HER activities of previous metal catalysts.

Catalysts	Electrolyte	Overpotential @10 mA cm^{-2} (mV)	Catalyst loading	Reference
Rh/NHCSs	**0.5 M H_2SO_4**	**7**	**0.6369 mg cm^{-2}**	**This work**
	1 M KOH	**6**		
	1.0 M PBS	**10**		
Ru@NC	0.5 M H_2SO_4	55.7	0.85 mg cm^{-2}	7
	1 M KOH	25.3		
	1.0 M PBS	165		
RuP_2@NPC	0.5 M H_2SO_4	38	1.0 mg cm^{-2}	8
	1 M KOH	52		
	1.0 M PBS	57		
Rh_2P	0.5 M H_2SO_4	14	0.15 mg cm^{-2}	9
	1 M KOH	30		
	1.0 M PBS	38		
Ru@C_2N	0.5 M H_2SO_4	13.5	0.285 mg cm^{-2}	10
	1 M KOH	17		
Rh_2P@NC	0.5 M H_2SO_4	9	0.7 mg cm^{-2}	11
	1 M KOH	10		
	1.0 M PBS	46		
Ru_2P/RGO-20	0.5 M H_2SO_4	22	1.0 mg cm^{-2}	12
	1 M KOH	13		
RuCoP	0.5 M H_2SO_4	11	0.06 mg_{Ru} cm^{-2}	13
	1 M KOH	23		
Ru NW	0.5 M H_2SO_4	15	0.202 mg cm^{-2}	9
	1 M KOH	38		
PtRu/CC1500	0.5 M H_2SO_4	8	$13.9_{Ru}/1.6_{Pt}$ μg cm^{-2}	14
	1 M PBS	25		
	1 M KOH	19		
Pt@mh-3D MXene	0.5 M H_2SO_4	12	0.2 mg cm^{-2}	15
	1 M KOH	31		
Pt-Ni/NiS NWs	0.5 M H_2SO_4	23	15.3 μg_{Pt} cm^{-2}	16
	1 M KOH	51		
Ru/NG-750	0.5 M H_2SO_4	53	0.102 mg cm^{-2}	17
	1 M KOH	8		
NiRu@N-C	0.5 M H_2SO_4	50	0.273 mg cm^{-2}	18
	1.0 M KOH	32		
Co_2P/Co_3O_4	1.0 M KOH	162	0.285 mg cm^{-2}	19
$Ni_{0.3}Co_{0.7}$-9AC-AD/NF	1.0 M KOH	143	/	20
C_{60}-$SWCNT_{15}$	0.5 M H_2SO_4	320	1.96 mol/L	21
	0.1 M KOH	380		
	1.0 M PBS	330		

CoFe-LDH@g-C_3N_4	1.0 M KOH	417	0.56 mg cm^{-2}	22
NiVB/rGO	0.5 M H_2SO_4 1.0 M KOH	146 151	0.56 mg cm^{-2}	23
CoMn-LDH@g-C_3N_4	1.0 M KOH	417	0.56 mg cm^{-2}	24
Pt_1/N-C	0.5 M H_2SO_4 1.0 M NaOH	19 46	~0.25 mg cm^{-2}	25
Ru-MoS_2/CC	1.0 M KOH	41	46 μg_{Ru} cm^{-2}	26
SA-Ru-MoS_2	1.0 M KOH	76	0.285 mg cm^{-2}	27
Ru/Fe–N–C	1.0 M KOH	9	0.485 mg cm^{-2}	28

Table S4. Mass activity values for the Ru/NHCSs, Rh/NHCSs and Ir/NHCSs.

Catalysts	1.0 M KOH	1.0 M PBS	0.5 M H_2SO_4
Ru/NHCSs	318.3 A g^{-1}	344.5 A g^{-1}	216.3 A g^{-1}
Rh/NHCSs	1348.5 A g^{-1}	564.5 A g^{-1}	1169.9 A g^{-1}
Ir/NHCSs	187.7 A g^{-1}	281.3 A g^{-1}	230.7A g^{-1}

Table S5. TOF values for the Ru/NHCSs, Rh/NHCSs and Ir/NHCSs.

Catalysts	1.0 M KOH	1.0 M PBS	0.5 M H_2SO_4
Ru/NHCSs	0.06 s^{-1}	0.05 s^{-1}	0.03 s^{-1}
Rh/NHCSs	1.42 s^{-1}	0.44 s^{-1}	0.91 s^{-1}
Ir/NHCSs	0.29 s^{-1}	0.41 s^{-1}	0.28 s^{-1}

References:

1. Y. Zhao, T. Ling, S. Chen, B. Jin, A. Vasileff, Y. Jiao, L. Song, J. Luo and S.-Z. Qiao, *Angewandte Chemie International Edition*, 2019, **58**, 12252-12257.
2. C. C. L. McCrory, S. Jung, J. C. Peters and T. F. Jaramillo, *Journal of the American Chemical Society*, 2013, **135**, 16977-16987.
3. M. S. Burke, M. G. Kast, L. Trotochaud, A. M. Smith and S. W. Boettcher, *Journal of the American Chemical Society*, 2015, **137**, 3638-3648.
4. F. Li, M. Han, Y. Jin, L. Zhang, T. Li, Y. Gao and C. Hu, *Applied Catalysis B: Environmental*, 2019, **256**, 117705.
5. H. Zhao, J. Ye, W. Song, D. Zhao, M. Kang, H. Shen and Z. Li, *ACS Applied Materials & Interfaces*, 2020, **12**, 6991-7000.
6. W. Ren, L. Xiong, G. Nie, H. Zhang, X. Duan and S. Wang, *Environmental Science & Technology*, 2020, **54**, 1267-1275.
7. J. Yang, H. Guo, S. Chen, Y. Li, C. Cai, P. Gao, L. Wang, Y. Zhang, R. Sun, X. Niu and Z. Wang, *Journal of Materials Chemistry A*, 2018, **6**, 13859-13866.
8. Z. Pu, I. S. Amiinu, Z. Kou, W. Li and S. Mu, *Angewandte Chemie International Edition*, 2017, **56**, 11559-11564.
9. F. Yang, Y. Zhao, Y. Du, Y. Chen, G. Cheng, S. Chen and W. Luo, *Advanced Energy Materials*, 2018, **8**, 1703489.
10. J. Mahmood, F. Li, S.-M. Jung, M. S. Okyay, I. Ahmad, S.-J. Kim, N. Park, H. Y. Jeong and J.-B. Baek, *Nat. Nanotechnol.* , 2017, **12**, 441-446.
11. Z. Pu, I. S. Amiinu, D. He, M. Wang, G. Li and S. Mu, *Nanoscale*, 2018, **10**, 12407-12412.
12. T. Liu, S. Wang, Q. Zhang, L. Chen, W. Hu and C. M. Li, *Chemical Communications*, 2018, **54**, 3343-3346.
13. J. Xu, T. Liu, J. Li, B. Li, Y. Liu, B. Zhang, D. Xiong, I. Amorim, W. Li and L. Liu, *Energy & Environmental Science*, 2018, **11**, 1819-1827.
14. L. Li, G. Zhang, B. Wang, T. Yang and S. Yang, *Journal of Materials Chemistry A*, 2020, **8**, 2090-2098.
15. L. Xiu, W. Pei, S. Zhou, Z. Wang, P. Yang, J. Zhao and J. Qiu, *Advanced Functional Materials*, **n/a**, 1910028.
16. P. Wang, X. Zhang, J. Zhang, S. Wan, S. Guo, G. Lu, J. Yao and X. Huang, *Nature Communications*, 2017, **8**, 14580.
17. R. Ye, Y. Liu, Z. Peng, T. Wang, A. S. Jalilov, B. I. Yakobson, S.-H. Wei and J. M. Tour, *ACS Applied Materials & Interfaces*, 2017, **9**, 3785-3791.
18. Y. Xu, S. Yin, C. Li, K. Deng, H. Xue, X. Li, H. Wang and L. Wang, *J. Mater. Chem. A*, 2018, **6**, 1376-1381.
19. J. Liu, D. Zhu, Y. Zheng, A. Vasileff and S.-Z. Qiao, *ACS Catal.* , 2018, **8**, 6707-6732.
20. W. Ye, Y. Yang, X. Fang, M. Arif, X. Chen and D. Yan, *ACS Sustainable Chemistry & Engineering*, 2019, **7**, 18085-18092.
21. R. Gao, Q. Dai, F. Du, D. Yan and L. Dai, *Journal of the American Chemical Society*, 2019, **141**, 11658-11666.
22. M. Arif, G. Yasin, M. Shakeel, M. A. Mushtaq, W. Ye, X. Fang, S. Ji and D. Yan, *Materials*

Chemistry Frontiers, 2019, **3**, 520-531.

23. M. Arif, G. Yasin, M. Shakeel, M. A. Mushtaq, W. Ye, X. Fang, S. Ji and D. Yan, *Journal of Energy Chemistry*, 2021, **58**, 237-246.
24. M. Arif, G. Yasin, M. Shakeel, X. Fang, R. Gao, S. Ji and D. Yan, *Chemistry – An Asian Journal*, 2018, **13**, 1045-1052.
25. S. Fang, X. Zhu, X. Liu, J. Gu, W. Liu, D. Wang, W. Zhang, Y. Lin, J. Lu, S. Wei, Y. Li and T. Yao, *Nature Communications*, 2020, **11**, 1029.
26. D. Wang, Q. Li, C. Han, Z. Xing and X. Yang, *Applied Catalysis B: Environmental*, 2019, **249**, 91-97.
27. J. Zhang, X. Xu, L. Yang, D. Cheng and D. Cao, *Small Methods*, 2019, **3**, 1900653.
28. C. Hu, E. Song, M. Wang, W. Chen, F. Huang, Z. Feng, J. Liu and J. Wang, *Advanced Science*, 2021, **8**, 2001881.